Dynamics and Morphology of Brittle Cracks: A Molecular-Dynamics Study of Silicon Nitride

Aiichiro Nakano, Rajiv K. Kalia, and Priya Vashishta

Concurrent Computing Laboratory for Materials Simulations, Department of Computer Science, Department of Physics and Astronomy, Louisiana State University, Baton Rouge, Louisiana 70803

(Received 5 May 1995)

Crack propagation in amorphous Si_3N_4 films is investigated with large-scale molecular-dynamics simulations on parallel machines. We observe a correlation between the speed of crack propagation and the morphology of fracture surfaces. Initially, as the crack propagates slowly, the roughness exponent for fracture surfaces is found to be 0.44. However, beyond a certain speed of crack propagation, the exponent crosses over to 0.8. This crossover behavior is similar to the recent experimental finding by Bouchaud and Navéos.

PACS numbers: 61.43.Bn, 61.20.Ja, 62.20.Mk

The morphology of fracture surfaces has drawn a great deal of attention in recent years. It is now well established that a fracture surface $z(x, y)$ is a self-affine object in that it remains invariant under the transformation $(x, y, z) \rightarrow (ax, ay, a_z^\alpha)$, where α is known as the roughness exponent. A decade ago, Mandelbrot and coworkers reported the first measurements of the roughness exponent for metallic surfaces [1]. Since then there has been a great deal of controversy regarding the value of α. Bouchaud, Lapasset, and Planès carried out measurements of α for four aluminum alloys with different heat treatments, and in each case they obtained $\alpha = 0.8$ [2]. Måløy *et al.* made measurements on six different brittle materials and found α to be 0.87 ± 0.07 [3]. This led them to conjecture that fracture surfaces of brittle and ductible materials had a "universal" roughness exponent, independent of material characteristics and the mode of fracture. Milman *et al.* questioned the validity of the "universality" of α, especially at microscopic length scales, by pointing out that their scanning tunneling microscopy data for MgO, Si, and Cu revealed the roughness exponent to be around 0.6 [4]. Measurements on tungsten and graphite also indicated a low value of α ($\approx$0.4) [4]. However, recent molecular-dynamics (MD) simulations for such disparate systems as porous silica [5] and two-dimensional Lennard-Jonesium [6] found $\alpha \approx 0.8$.

In this Letter we report the results of a MD study of crack propagation and the morphology of fracture surfaces in amorphous silicon nitride films. In these films, we find the primary crack propagates slowly at a speed of 640 m/s for the first 12.1 ps of the MD simulation and the corresponding fracture surfaces have a roughness exponent of 0.44. After 12.1 ps we observe considerable secondary fracture ahead of the primary crack, with the crack accelerating to a speed of 1630 m/s. The resulting fracture surfaces of the amorphous film are found to have a much higher value ($= 0.82$) of the roughness exponent. Such a crossover behavior has also been observed in a recent experiment by Bouchaud and Navéos [7], and it is consistent with a model in which a fracture surface is considered the trace of a line propagating in a random medium [8]. The model predicts the roughness exponent to be 0.75 for high-velocity and 0.5 for low-velocity fracture surfaces [9].

MD study of fracture in Si_3N_4 films involved systems with 100 352 atoms (typical dimensions of a film were $220 \times 220 \times 20\,\text{Å}^3$), interacting via a combination of two- and three-body potentials. The two-body potential includes steric repulsion, the effect of charge transfer via Coulomb interaction, and the large electronic polarizability of anions through the charge-dipole interaction [10]. Three-body interactions with bond-bending and bond-stretching terms were introduced to include covalent effects [10]. Using highly efficient multiresolution algorithms [11], the MD simulations were performed on the 128-node IBM SP computer at Argonne National Laboratory. (This MD implementation has a parallel efficiency of 92%, communication overhead of only 8%, and it executes a 4.2×10^6 particle simulation of Si_3N_4 at the rate of 10.3 s per time step on 64 nodes.)

To evaluate the quality of the interaction scheme, various structural and dynamical correlations and elastic constants in the bulk Si_3N_4 were computed and the results were compared with available experimental measurements

TABLE I. Elastic moduli of α-Si_3N_4. The MD results for the hydrostatic bulk modulus β_v^{-1}, the inverse linear compressibilities parallel to the a and c axes β_a^{-1} and β_c^{-1}, and the elastic moduli along the directions with angles 5°, 64.2°, and 83.1° from the c axis are compared with experiments.

	MD (GPa)	Experiment (GPa)
β_v^{-1}	287	282[a]
β_a^{-1}	824	847[a]
β_c^{-1}	943	870[a]
$E(5°)$	419	456[b]
$E(64.2°)$	375	378[b]
$E(83.1°)$	386	488[b]

[a]Reference [12].

[b]Reference [13].

 0031-9007/95/75(17)/3138(4)$06.00

[10]. In the crystalline state, the MD results for interparticle separations (Si-Si, Si-N, and N-N) and bond angle distributions (N-Si-N and Si-N-Si) are in excellent agreement with experiments. Not only that, the MD static structure factor for the glass agrees well with neutron-scattering measurements over the entire range of wave vectors. The specific heat of crystalline α-Si_3N_4, obtained from the phonon density of states, is also in excellent agreement with experimental measurements over a wide range of temperatures. The MD results for various elastic moduli are also in reasonable agreement with experimental values [12,13]; see Table I.

As a precursor to the study of crack propagation in Si_3N_4, we investigated the response of well-thermalized crystalline and amorphous films to uniaxial tensile loads. Crystalline films were obtained by removing periodic boundary conditions on well-thermalized bulk α-Si_3N_4 crystals and then relaxing the systems with MD and conjugate-gradient schemes. (The a and c axes were parallel to the x and z axes, respectively, and the film was perpendicular to the z axis.) In the case of amorphous films, we first prepared well-thermalized bulk systems by quenching the molten state and then periodic boundary conditions were removed and the systems were relaxed with MD and conjugate-gradient methods. These well-thermalized crystalline and amorphous Si_3N_4 films were subjected to uniaxial tensile loads by displacing atoms uniformly in the uppermost and lowermost layers (thickness ~5.5 Å each) along the x direction. The strain was applied at a constant rate while maintaining the temperature at 300 K.

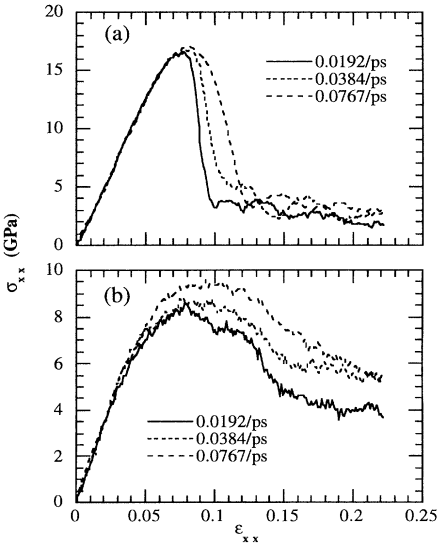

FIG. 1. Tensile stress σ_{xx}, in the x direction as a function of the uniaxial strain ε_{xx} in the x direction for (a) α-crystal and (b) amorphous Si_3N_4 films at various strain rates between 0.0192 and 0.0767 ps^{-1}.

Figure 1 shows the strain-stress curves for crystalline and amorphous films at various strain rates between 0.0192 and 0.0767 ps^{-1}. The response of crystalline films to tensile strain follows Hooke's law until the strain reaches a critical value of ~8% where the films fail catastrophically [see Fig. 1(a)]. In the case of amorphous films, Fig. 1(b) shows that the peak in the strain-stress curve, i.e., the theoretical tensile strength without macroscopic defects, is much smaller than that for crystalline films. Furthermore, in amorphous films Hooke's law applies over a much narrower range than in crystalline films because of the presence of microstructures. Outside the regimes where Hooke's law applies, the strain-stress curves exhibit a strong strain-rate dependence due to the slow rearrangement of SiN_4 tetrahedral units [14].

The difference between the strain-stress curves of the crystalline and amorphous films results from different microstructures in these systems. Figure 2 shows 5.6-Å-thick slices of α-crystal and amorphous films before failure (strain ~3.3%). Crystalline films respond to tensile load by uniformly rearranging the tetrahedral units [see Fig. 2(a)] whereas in amorphous films micropores develop and they coalesce to release the stress [see Fig. 2(b)].

To investigate crack propagation in an amorphous Si_3N_4 film by MD simulations [15], we insert a crack in a uniaxially stretched film (strain ~4%) by removing particles within a region whose projection onto the xy plane is 4×50 $Å^2$, and we use a strain rate of 0.01 ps^{-1}. The crack plane is parallel to the yz plane, and the crack propagates along the y direction.

Figure 3 shows snapshots of the amorphous Si_3N_4 film projected onto the xy plane. Initially the crack propagates straight along the y direction, as shown in Fig. 3(a), for the first 4.5 ps. At 9.7 ps, we observe the formation of voids in front of the crack tip [see Fig. 3(b)]. These voids grow and form a secondary crack, and eventually the secondary crack and the primary crack coalesce, as shown in Fig. 3(c) at 12.3 ps. The resulting crack surface is very rough, as evident from the snapshot in Fig. 3(d) at $t = 16.4$ ps.

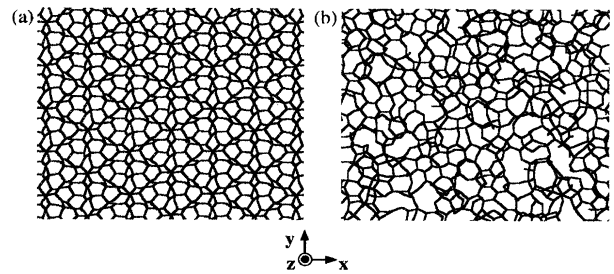

FIG. 2 (color). 5.6-Å-thick slices of (a) α-crystal and (b) amorphous Si_3N_4 films under 3.3% uniaxial strain. Lines represent Si-N bonds. The cyan and magenta colors represent bonds emanating from Si and N atoms, respectively. The figures show film segments (39×36 Å).

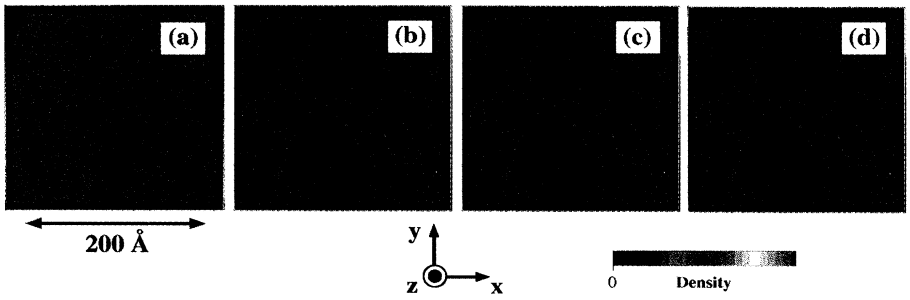

FIG. 3 (color). Snapshots of crack propagation in an amorphous Si_3N_4 film at time (a) 4.5 ps, (b) 9.7 ps, (c) 12.3 ps, and (d) 16.4 ps. The color code represents the particle density. These figures show the formation and coalescence of secondary cracks.

We have calculated the height-height correlation function [5]

$$g(y) = \langle [h(y + y_0) - h(y_0)]^2 \rangle^{1/2} \quad (1)$$

of the crack surface using the height profile $h(y)$. In Eq. (1), the bracket denotes the average over y_0. For a self-affine surface, the height-height correlation function is expected to obey the scaling relation $g(y) \sim y^{\alpha}$ [1–4,16].

Figure 4 shows a log-log plot of the height-height correlation function for the crack surface in the amorphous film. There are two well-delineated regimes in this figure. For smaller length scales, we observe a rather smooth crack surface with a smaller roughness exponent. By linear fitting we obtain a roughness exponent of 0.44 ± 0.02 for $y < \xi < 25$ Å. Beyond this crossover length ξ, the surface is rougher with a larger exponent $\alpha = 0.82 \pm 0.02$.

To relate the morphology of the crack surface to the crack dynamics, we show in Fig. 5 the crack tip position as a function of time in the amorphous film. Initially the crack propagates slowly and continuously. At 12.1 ps the crack tip jumps suddenly as the primary and secondary cracks coalesce. The distances between this and each of the subsequent jumps are between 20 and 40 Å, which are close to the crossover length of the height-height correlation function. We thus conclude that the smaller roughness exponent ($\alpha = 0.44$) corresponds to slow crack propagation inside microcracks, and the larger exponent ($\alpha = 0.82$) corresponds to the intermicrocrack propagation associated with the coalescence of microcracks [17]. The average propagation speed in the second regime (1630 m/s) is much larger than in the first regime (640 m/s).

The above conclusion is further confirmed by the calculation of the intramicrocrack height-height correlation function. Before the primary and secondary cracks coalesce, $g(y)$ is calculated separately for the two cracks at 12.0 ps. The results are then averaged as shown in the inset of Fig. 4, and we obtain a roughness exponent $\alpha = 0.40 \pm 0.04$, corresponding to intramicrocrack propagation. This result is close to the smaller exponent ($\alpha = 0.44$) of the fracture surface.

A similar crossover from quasistatic to rapid fracture was observed in recent experiments by Bouchaud and Navéos [7]. For titanium aluminum alloys, they observed a crossover of the roughness exponent from 0.45 to 0.84. They also found that the crossover length scale decreases when the local stress intensity factor, or correlatively, the

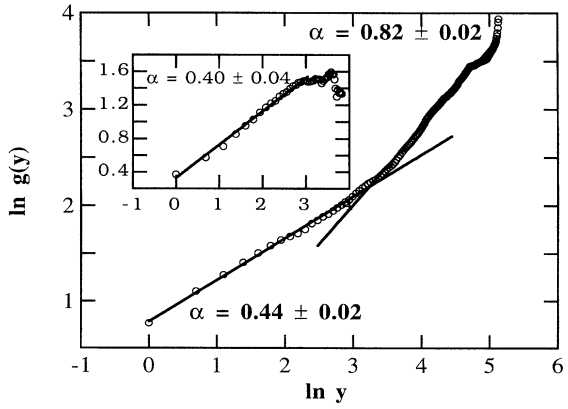

FIG. 4. Log-log plot of the height-height correlation function $g(y)$ (open circles). The solid lines represent the best fit $g(y) \sim y^{\alpha}$, with $\alpha = 0.44 \pm 0.02$ for $y < \xi = 25$ Å, and $\alpha = 0.82 \pm 0.02$ for $y > \xi$. The inset shows $g(y)$ (open circles) within the primary and secondary cracks at 12.0 ps before they coalesce. The best fit (solid line) gives $\alpha = 0.40 \pm 0.04$.

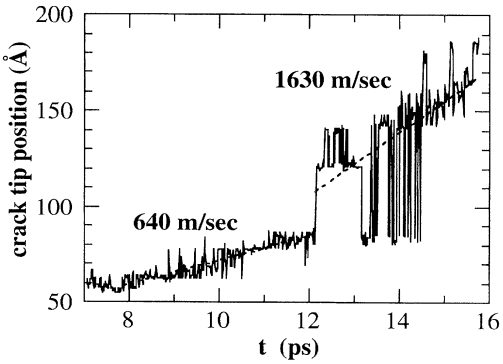

FIG. 5. Crack tip position as a function of time (solid curves) in an amorphous Si_3N_4 film. Linear fits (dashed lines) before and after 12.1 ps give the average crack tip velocities of 640 and 1630 m/s, respectively.

crack velocity increases. In MD simulations, the very large tensile stress results in a small crossover length on the nanometer scale.

This crossover phenomenon is consistent with a model in which a fracture surface is considered the trace of a line propagating in a random medium [7,8]. The model predicts the roughness exponent to be 0.75 for high-velocity and 0.5 for low-velocity fracture surfaces [9].

In summary, we have observed a crossover from slow to rapid fracture in MD simulations of amorphous silicon nitride films. The morphology of the crack surfaces correlates with the crack dynamics: The slow propagation creates smooth crack surfaces with a roughness exponent of 0.44; on the other hand, the rapid propagation creates rough surfaces with an exponent of 0.82. This crossover behavior is in agreement with recent experiments by Bouchaud and Navéos [7].

This work was supported by U.S. Department of Energy Grant No. DE-FG05-92ER45477, National Science Foundation Grant No. DMR-9412965, and Air Force Office of Scientific Research Grant No. F 49620-94-1-0444. A part of these simulations were performed on the 128-node IBM SP computer at Argonne National Laboratory. The computations were also performed on parallel machines in the Concurrent Computing Laboratory for Materials Simulations (CCLMS) at Louisiana State University. The facilities in the CCLMS were acquired with the Equipment Enhancement Grants awarded by the Louisiana Board of Regents through Louisiana Education Quality Support Fund.

[1] B. B. Mandelbrot, D. E. Passoja, and A. J. Paullay, Nature (London) **308**, 721 (1984).

[2] E. Bouchaud, G. Lapasset, and J. Planès, Europhys. Lett. **13**, 73 (1990); E. Bouchaud, G. Lapasset, J. Planès, and S. Navéos, Phys. Rev. B **48**, 2917 (1993).

[3] K. J. Måløy, A. Hansen, E. L. Hinrichsen, and S. Roux, Phys. Rev. Lett. **68**, 213 (1992); **71**, 205 (1993).

[4] V. Y. Milman, R. Blumenfeld, N. A. Stelmashenko, and R. C. Ball, Phys. Rev. Lett. **71**, 204 (1993).

[5] A. Nakano, R. K. Kalia, and P. Vashishta, Phys. Rev. Lett. **73**, 2336 (1994).

[6] F. F. Abraham, D. Brodbeck, R. A. Rafey, and W. E. Rudge, Phys. Rev. Lett. **73**, 272 (1994).

[7] E. Bouchaud and S. Navéos (to be published).

[8] J. P. Bouchaud, E. Bouchaud, G. Lapasset, and J. Planès, Phys. Rev. Lett. **71**, 2240 (1993).

[9] D. Etras and M. Karder, Phys. Rev. Lett. **69**, 889 (1992).

[10] P. Vashishta, R. K. Kalia, and I. Ebbsjö, Phys. Rev. Lett. (to be published); A. Omeltchenko, A. Nakano, R. K. Kalia, and P. Vashishta (to be published).

[11] R. K. Kalia, S. W. de Leeuw, A. Nakano, D. L. Greenwell, and P. Vashishta, Comput. Phys. Commun. **74**, 316 (1993); A. Nakano, P. Vashishta, and R. K. Kalia, *ibid.* **77**, 302 (1993); A. Nakano, R. K. Kalia, and P. Vashishta, *ibid.* **83**, 197 (1994).

[12] L. Cartz and J. D. Jorgensen, J. Appl. Phys. **52**, 236 (1981).

[13] A. A. Mukaseev, V. N. Gribkov, B. V. Shchetanov, A. S. Isaikin, and V. A. Silaev, Poroshk. Metall. **12**, 97 (1972).

[14] R. Ochoa, T. P. Swiler, and J. H. Simmons, J. Non-Cryst. Solids **128**, 57 (1991).

[15] Microscopic mechanisms of crack propagation in two-dimensional and bulk crystalline systems have been studied by MD simulations in Refs. [6] and [18–20].

[16] At vertical coordinate y the height profile $h(y)$ is calculated as the largest (smallest) horizontal coordinate of the lower (upper) crack surface in the x direction. Because of small system size, it is difficult to establish self-affinity and associated correlation length. However, the exponent α is useful to quantify the surfaces at different length scales.

[17] It should be noted that disorder plays an important role in the observed crossover behavior. In MD simulations on crystalline films, we found that cracks propagate straight along the y direction in a cleavage manner. Because of a dynamic instability, higher crack velocities have been shown to lead to rougher fracture surfaces even in crystals [6] and homogeneous materials [21]. We are performing simulations for large crystalline films to investigate the nature of such a dynamic instability.

[18] W. T. Ashurst and W. G. Hoover, Phys. Rev. B **14**, 1465 (1976).

[19] A. Paskin, A. Gohar, and G. J. Dienes, Phys. Rev. Lett. **44**, 940 (1980).

[20] K. S. Cheung and S. Yip, Phys. Rev. Lett. **65**, 2804 (1990).

[21] J. Fineberg, S. P. Gross, M. Marder, and H. L. Swinney, Phys. Rev. Lett. **67**, 457 (1991).

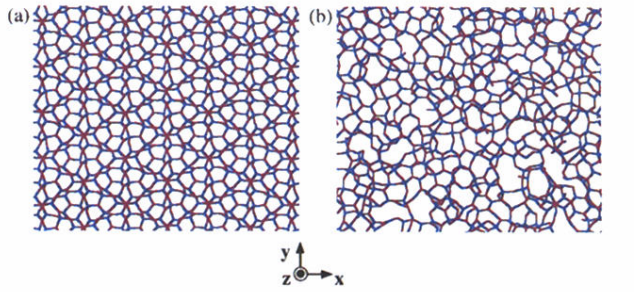

FIG. 2 (color). 5.6-Å-thick slices of (a) α-crystal and (b) amorphous Si_3N_4 films under 3.3% uniaxial strain. Lines represent Si-N bonds. The cyan and magenta colors represent bonds emanating from Si and N atoms, respectively. The figures show film segments (39×36 Å).

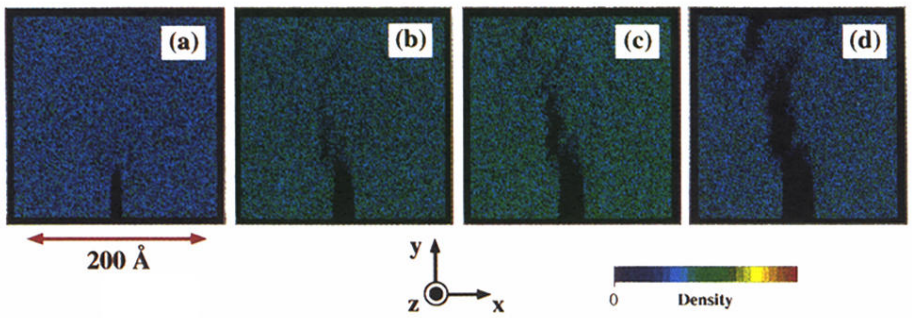

FIG. 3 (color). Snapshots of crack propagation in an amorphous Si_3N_4 film at time (a) 4.5 ps, (b) 9.7 ps, (c) 12.3 ps, and (d) 16.4 ps. The color code represents the particle density. These figures show the formation and coalescence of secondary cracks.